

Environmental dependence of atomic-scale friction at graphite surface steps

Philip Egberts,¹ Zhijiang Ye,² Xin Z. Liu,¹ Yalin Dong,³ Ashlie Martini,^{2,*} and Robert W. Carpick^{1,†}

¹*Department of Mechanical Engineering and Applied Mechanics, University of Pennsylvania, 220 South 33rd Street, Philadelphia, Pennsylvania 19104, USA*

²*School of Engineering, University of California Merced, 5200 North Lake Road, Merced, California 95343, USA*

³*School of Mechanical Engineering, Purdue University, 585 Purdue Mall, West Lafayette, Indiana 47907, USA*

(Received 24 January 2013; revised manuscript received 14 June 2013; published 3 July 2013)

Atomic force microscopy experiments and molecular dynamics simulations show that friction between a nanoscale tip and atomically stepped surfaces of graphite is influenced by the environment. The presence of a small amount of water increases friction at atomic steps, but does not strongly influence friction on flat terraces.

DOI: [10.1103/PhysRevB.88.035409](https://doi.org/10.1103/PhysRevB.88.035409)

PACS number(s): 68.35.Af, 02.70.Ns, 62.20.Qp, 68.37.Ps

I. INTRODUCTION

Since the first observation of atomic lattice-resolved friction,¹ there has been considerable interest in understanding the physical origins of friction and mechanisms of frictional dissipation at the atomic scale.^{2,3} As that first result, which was obtained for a nanoscale tip sliding on the surface of a highly oriented pyrolytic graphite (HOPG) sample, most experiments, simulations, and theoretical studies have focused on ideal, atomically flat surfaces;^{2,4,5} such idealizations may not reflect the topography of many practical surfaces. A specific example of a nonideal feature ubiquitous to crystal surfaces is a step edge. It has been found that lateral forces change locally when nanoscale tips slide across step edges.^{6–11} In atomic-scale studies of surface steps, the chemistry and stability of atomic steps are strongly influenced by the environment. For example, atomic steps on ionic crystals become mobile in the presence of water vapor.¹² Although not mobile, the chemical potential of atoms at HOPG steps are also strongly influenced by the environment.¹³ Thus, the environment could significantly affect friction. Furthermore, recent studies have shown that atomic friction on flat surfaces is also strongly influenced by the presence of water through the formation of a meniscus at the tip-sample contact,¹⁴ suggesting that the environment could also influence the friction force occurring at atomic steps and other defects. However, clear evidence for this has not yet been established in the literature: In two specific atomic friction studies of steps on HOPG, enhanced friction at surface steps was observed in both humid air⁹ and ultrahigh vacuum (UHV),⁸ despite the different environmental conditions. In addition, the environment strongly affects the wear of graphite at macroscopic scales;¹⁵ links to nanoscale behavior to explain this are lacking.

In this paper, we address the influence of the environment on atomic-scale friction to understand the mechanisms that govern friction at step edges, on HOPG surfaces, and to address seemingly divergent literature results of atomic-scale studies at step edges where friction behavior was independent of the environment. Atomic friction is examined on stepped surfaces of HOPG using an atomic force microscope (AFM) complemented by fully atomistic molecular dynamics (MD) simulations in a system that has been matched in terms of sample material, tip size, compliance, and the presence or absence of adsorbates. Comparison between simulation and experiment enables a more complete understanding of the

lateral force response. HOPG is deliberately chosen here as it has well-established atomic potentials, required for reliable MD simulations, and has a stable surface structure in UHV and humid air, allowing for a time-invariant analysis of the frictional behavior of steps in different environments.

II. METHODS

A. AFM experiments

All experiments were conducted in a RHK 750 UHV-AFM system in either ultrapure dry nitrogen or high vacuum (HV) conditions at room temperature. Samples of HOPG were cleaved in laboratory air. Given the humidity 30–60% of the laboratory air, water is expected to adsorb on the graphite surface, particularly at step edges.^{13,16,17} The samples were then placed in the fast entry lock of the UHV system, which was filled with N₂ vapor, and then sealed, all within a few minutes. Subsequently, the HOPG sample was transferred into the N₂-purged AFM chamber, where friction experiments were conducted within the next 6 h. The N₂ gas used to fill the chamber was obtained from vapor extracted from a liquid nitrogen dewar, achieving a highly pure nitrogen environment of <2% relative humidity based on measurements taken under the same conditions in a similar UHV chamber. Following these measurements, the chamber was pumped down for 12 h, achieving a base pressure of $\sim 2 \times 10^{-7}$ Torr. Friction experiments were then repeated under these conditions on the same sample and in a similar area as measured previously. Figure 1 shows an x-ray photoelectron spectroscopy (XPS) survey spectra of the HOPG surface acquired under HV conditions. Under these conditions, no water is detected on the surface, as is evident in the inset of Fig. 1 that highlights the binding energies where water is found. This demonstrates that adsorbed water was able to desorb under the HV conditions, to within the detection limit of the XPS instrument. Furthermore, no water was detected in XPS measurements acquired on Ag surfaces at 0.4 Torr exposed to the same N₂ gas if the sample had been exposed to HV conditions for several hours beforehand,¹⁸ demonstrating the low water content of the N₂ gas. However, as we will discuss further below, all evidence indicates that when water has been preadsorbed onto surfaces due to air exposure, a significant amount remains while the sample is held in N₂ gas; HV exposure is required to desorb a significant fraction of water from the HOPG surface.

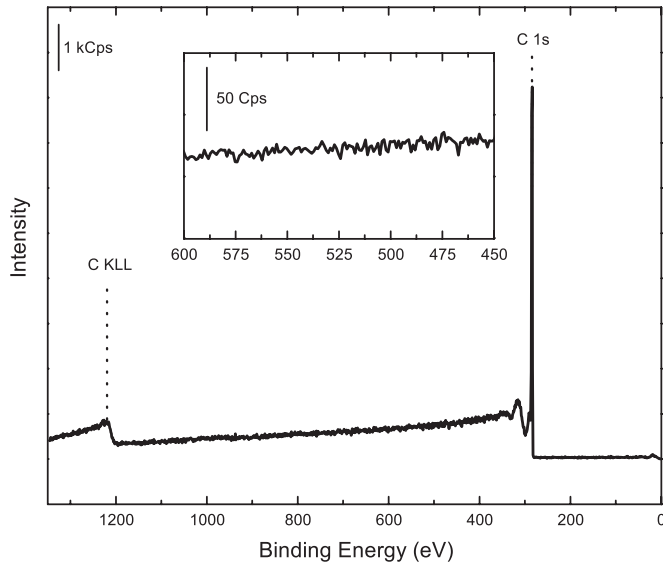


FIG. 1. XPS survey spectra of freshly cleaved clean graphite using the XPS system described in Ref. 18 measured in HV conditions. No water is present within the detection limits of our XPS system, which is 0.1 atomic percent. Should water be present, a peak at a binding energy of 534 eV would be visible.

Following friction measurements, *post-mortem* transmission electron microscopy (TEM) (JEOL 2010F) imaging of the tip apex was performed. The radius of the lowest protrusion was then estimated from the TEM images by tracing the contacting asperity of the tip (accounting for the 22.5° tilt of the cantilever with respect to the sample surface in the AFM) and then fitting a circle to the traced profile.¹⁹ This protocol was repeated three times with three different AFM probes, all producing consistent results.

Silicon cantilevers with an integrated tip (Nanosensors PPP-CONT) were used as force sensors. The normal bending and lateral twisting spring constants of the force sensor were determined under N_2 conditions using the Sader method,²⁰ yielding normal spring constants between 0.01 and 0.2 N/m and torsional spring constants between 10 and 120 N/m. The optical sensitivity of the quadrant detector was assumed to be the same in both lateral and normal directions, and was determined by measuring the slope of the cantilever normal bending signal versus sample displacement in the z direction. As usual, lateral forces correspond to the measured twisting signal of the cantilever converted to a force. Friction forces were taken as the local average hysteresis between the lateral forces in the forward and reverse scanning directions. Thus, we are careful to distinguish between friction forces and lateral forces, the former corresponding to dissipative forces against which the tip must expend work to slide, and the latter being the net horizontal force the tip experiences at any point while sliding along the surface. Contributions affecting the lateral force include friction. This can result from static friction force during unstable stick-slip sliding, or kinetic friction forces during smooth sliding. In either case, these higher friction forces are manifested in hysteresis (a friction loop) in forward versus back lateral forces.

The load dependence of friction was always acquired in the following manner: (1) A force versus distance curve was acquired to determine the initial zero deflection or normal force value. (2) Friction forces were measured by initially ensuring the normal force corresponded to this initial zero deflection (i.e., zero externally applied load), and then increasing the normal force in small, defined increments to a maximum value. In later sections, we refer to friction measured in this manner as friction acquired during loading. (3) The friction forces were then measured while decreasing the normal force until the tip pulled out of contact from the surface. Friction measured during this stage will be later referred to as friction acquired during unloading. (4) A force versus distance curve was once again acquired to determine the zero deflection or force value. This value was then used while processing to account for any drift in the normal force that occurred between these two force curves. In all experiments, the lateral scanning speed was between 200 and 500 nm/s. Experimental data was processed using WSXM.²¹

B. MD simulations

The fully atomistic MD model mimicked the apex of an AFM tip scanning over a graphite step edge having a zigzag termination, and is graphically illustrated in Fig. 5(e). Although this termination affects electronic properties,²² these are not captured in atomistic simulations and, therefore, no edge termination effect on friction was observed in the simulations. Model hemispherical tips with radii between 2 and 8 nm consisting of carbon atoms in a diamond structure were used. To match the compliance of the AFM system, the tip was connected by a harmonic spring to a support. The spring stiffness was $k = 8$ N/m in the directions parallel to the plane of sliding. To scan, the support was moved laterally with a constant speed of 4 m/s. While this exceeds the experimental scan speed by seven orders of magnitude (a problem endemic to most AFM-MD studies), the model predictions are still meaningful. In previous work we showed that, although caution is required when comparing inertial or dynamic effects, the energetic parameters observed in MD simulations constructed with reliable potentials matched with AFM experiments.⁴ The top three layers of the tip acted as a rigid body on which a constant normal load was applied. The substrate consisted of three graphene layers with the bottom-most layer fixed. In some simulations, water molecules were placed in the vicinity of the tip-substrate contact. A Langevin thermostat was applied to all atoms whose positions were not constrained to maintain a simulation temperature of either 10 or 300 K. The boundaries were periodic in the sliding plane, and the boundary in the surface-normal direction was formed by the fixed bottom layer of the substrate and the rigid body of atoms at the top of the tip. Atoms within the tip and substrate interacted via the adaptive intermolecular reactive empirical bond order (AIREBO)²³ potential. The TIP4P potential was used for the water molecules,²⁴ and the Lennard-Jones potential was used to model interactions between graphite layers ($\epsilon = 0.00384$ eV, $\sigma = 0.34$ nm), between the tip and graphite ($\epsilon = 0.00384$ eV, $\sigma = 0.34$ nm), and between water molecules and the tip or substrate ($\epsilon = 0.006499$ eV, $\sigma = 0.319$ nm).

III. RESULTS

For all results, the forward sliding direction is always plotted from left to right, and the tip moves down (up) a step when sliding forward (reverse). The lateral force measured is positive (negative) when scanning in the forward (backward) direction. For all experimental data, we only consider monatomic steps that are within $\pm 30^\circ$ of being perpendicular direction of the fast scan direction in the AFM, which is always 90° to the long axis of the cantilever. This ensures that torsion is maximized and longitudinal bending or buckling of the cantilever is minimized when traversing a step. In simulations, this angle was fixed at 90° . However, no appreciable difference in friction was found when the tip traversed the step at angles between 60° and 90° .

A. Experimental results

Experiments in N_2 (cleaved in air, transferred to N_2 , no prior HV exposure; thus, some water will be present on the surface) and HV (cleaved in air, transferred to N_2 , then pumped to HV; thus, water has the opportunity to desorb—we denote this as the “clean” surface) yield two distinct trends in both the friction behavior and the peak lateral forces as the tip slides over the step. A typical friction loop for clean HOPG is illustrated in Fig. 2(a). In this case, the lateral forces at the step edge have the same polarity in the forward and reverse directions, resulting in relatively low friction. With water present, we observe a different behavior than on the clean surface [see Fig. 2(b)]. In this case, there is little observable change in the lateral force while sliding in the forward direction, but there is a significant change (increased resistance) in the reverse direction, resulting in additional friction at the step.

We term the friction behavior at a clean graphite step, such as in Fig. 2(a), the “geometry-dominated case.” The observed lateral force in the forward scan direction has a negative magnitude that results from an “assistive” force acting on the tip helping it to move down the step. In the reverse scan direction, an increased negative lateral force at the step edge results from additional resistance experienced by the tip as it moves up the step. This is all simply due to the tip’s interaction with the geometry of the step, which gives the normal force a component parallel to the sliding direction; this is essentially the same effect that alters lateral forces on sloped surfaces,²⁵ and has been discussed many times before in the context of atomic steps. Figure 2(c) shows the peak lateral force, defined as the value of the lateral force at its maximum magnitude in either the forward (step down) and reverse (step up) scan directions, as a function of the normal force at a step edge, on both surfaces. For clean surfaces, the slopes are similar for both step up (red squares) and step down (black squares). The result of friction measurements made on clean surfaces is best summarized by Fig. 2(d), which shows the variation of friction with normal force at steps and on terraces, on the clean surface, and with water present. On the clean surface, we observe higher friction at the step edge (blue squares) compared to terraces (green squares).

In the presence of water, friction loops typical of Fig. 2(b) are consistently obtained: The lateral force at the step is unchanging or slightly more positive during the forward scan (step down) and is more negative during the reverse scans (step up). Assuming the geometrical contribution to the lateral force

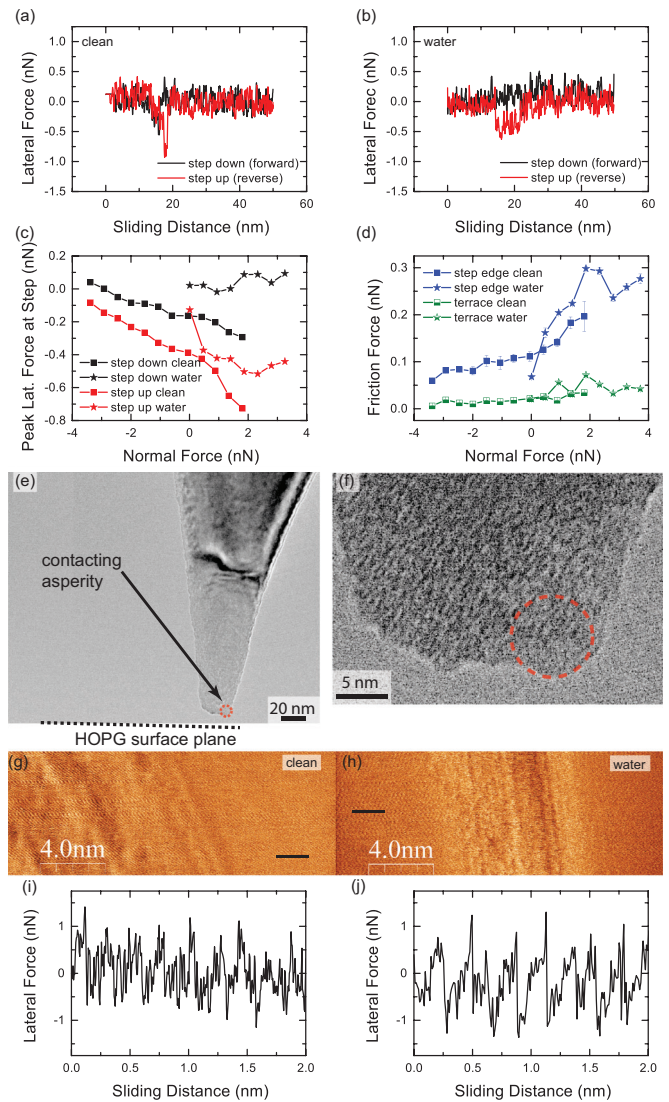


FIG. 2. (Color online) Experimental results of step friction on HOPG. Lateral force line profiles acquired on (a) clean surfaces (HV conditions, normal force = 0.98 nN) and (b) with water present (N_2 conditions without pumping, normal force = 0.94 nN). Red (black) data always indicate step-up (step-down) measurements. The load dependence of (c) the peak lateral force and (d) friction recorded at the step edge measured on both the clean surface and with water present using the same tip. Only unloading data is presented in (c) and (d). Error bars in (d) represent the 95% confidence interval. (e) TEM image of the tip used to obtain data shown in (a)–(d). (f) A higher magnification image of the tip apex, also identifying the contacting asperity. The fit of the end asperity is shown by the dashed red line. Lateral force image (forward) showing lattice resolution of the graphite surface at a single step on (g) the clean surface and (h) with water present. Note the color scale in (g) and (h) indicates that lateral forces are more positive (negative) in brighter (darker) regions. Black lines in (h) and (g) indicate regions where lateral force line profiles are shown in (i) and (j), respectively. A TEM image of the contacting asperity of the tip used to acquire (h) is shown in Fig. 6(b).

is independent of environment, these results show that with water present, there is much stronger (in fact, a dominating) frictional contribution that resists motion in both directions

compared to the clean surface. We therefore refer to this as the “dissipation-dominated” case.

Focusing on the variation of peak lateral forces with normal force, we observe trends that are consistent with previous reports on surfaces with water present,⁹ but also on clean surfaces.⁸ In Fig. 2(c), the peak lateral force in the step-down direction with water present (black stars) varies little with normal force, while the peak lateral force in the step-up direction (red stars) decreases strongly overall with increasing normal force. The net effect then is a significant increase in friction with normal force at the step when water is present. However, Fig. 2(c) shows that the peak lateral force in the step-up direction on the clean surface (red squares) and with water present (red stars) have a similar, negative slope, indicating that peak lateral forces in the step-up direction are primarily dominated by geometric contributions. Figure 2(d) shows that the friction at the step (blue stars) is higher and varies more strongly with normal force than the friction measured on the terrace (green stars). In addition, friction at step edges is larger with water present than on the clean surface for the cases where the tested loads coincide (with the exception of the data point near 0 nN normal force). Figure 3(a) shows fits of the unloading friction force versus normal force curves, which clearly demonstrates a reduction in the friction force on the clean surface, compared to when water was present.

This environmental dependence of friction behavior at steps was consistently observed for multiple tips having radii ranging from 4 to 40 nm. As well, the slope of the friction versus normal force data at steps is always larger when water is present compared with the clean case. Additionally, every time we examined single graphite steps with a new tip in vacuum, or in cases where the sample was stored in vacuum overnight

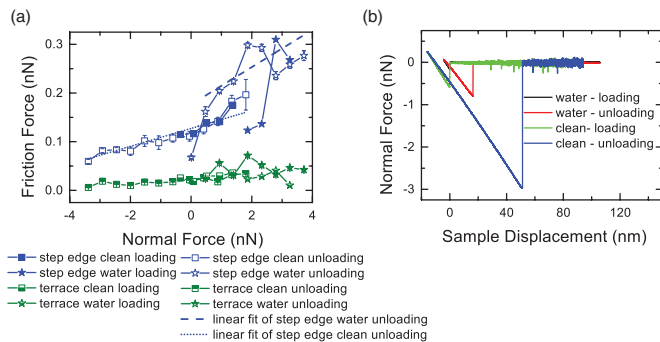


FIG. 3. (Color online) (a) Friction force vs normal force data from Fig. 1(d) showing the overlap of loading (solid and bottom-half solid data points) and unloading (open and top-half solid data points) curves. Note that the friction measured on the terrace with water present (dry nitrogen: green stars) and on the clean surface (HV: green squares) have the same values. However, the friction observed at the step edge with water (nitrogen: blue stars) is slightly higher than on the clean surface (HV: blue squares). Fits of the unloading data on the clean surface (blue dotted line) and when water was present (blue dashed line) are 0.018 ± 0.002 and 0.04 ± 0.01 , respectively. The fit determined on the surface with water was present was determined without the data point near 0 nN. (b) Force vs sample z -displacement curves taken with water present (nitrogen: red and black) and on the clean surface (HV: green and blue) show that the pull-off force has changed from -0.8 to -3.0 nN.

and then subsequently imaged in N_2 , the lateral force response at the atomic steps was geometry dominated (thus, with little friction enhancement). Given the sequence of environmental changes (i.e., measurements performed in N_2 conditions either before or after the sample had been exposed to HV conditions), we hypothesize that significant water desorption occurs once the sample is exposed to HV environments, but that desorption requires significant time when exposed to dry nitrogen due to the adsorption energy of water. Finally, despite an approximate threefold increase in pull-off force measured for experiments conducted in dry nitrogen when compared to those conducted in HV conditions [Fig. 3(b)], the variation of the friction force with normal force on a single graphite terrace does not change with the environment [as shown in Fig. 2(d)]. This result is in contrast to the increased friction observed at the step edge when changing from surfaces having water to a clean surface. These results support our hypothesis that exposure to a humid atmosphere predominantly affects friction at the steps.

Figure 2(e) shows the tip used for these measurements. The asperity (the lowest point on the tip) was identified geometrically in the TEM image and traced. The traced profile was fit with a circle and is shown in Fig. 2(f), yielding a radius of 4 ± 1 nm. Topographic imaging of the surface in both environments verifies the step height as a single atomic step. No evidence of tip wear was observed in topographic imaging (i.e., no change in the sharpness of the step edge feature). The absence of tip wear is further confirmed by the overlapping loading and unloading friction force versus normal force data [Fig. 3(a)] and is supported by the similarity of the step width observed in all topographic images, as well as the small size of the contacting asperity measured in *post-mortem* TEM images.

Finally, lattice resolution images are shown in Fig. 2 for the step-up direction, acquired both on the clean surface [Fig. 2(g)] and with water present [Fig. 2(h)], demonstrating the sensitivity we achieved in detecting lateral forces at step edges. Atomic stick slip can be clearly observed in the lateral force profiles in Figs. 2(i) and 2(j).

An example of the same measurement performed with a tip having a larger, 29 ± 1 nm, radius can be observed in Fig. 4. As in the case of Fig. 2, Fig. 4(a) shows that the load dependence of the peak lateral force follows the same trends observed for the smaller tip in Fig. 2(c). Figure 4(b) shows that the friction force at the step is far greater when water is present compared to the clean case. In addition, higher friction at steps compared to terraces is clearly seen (with the difference being much greater when water is present). Additionally, the loading and unloading curves are perfectly overlapping in both environments, also suggesting that no tip wear occurred during friction measurements with this particular tip. Finally, a TEM image of the tip apex is shown in Fig. 4(c), allowing for the determination of the tip radius. Four additional measurements carried out with four different tips are included in the Appendix, all showing similar trends for the friction behavior as that presented above. In particular, and as shown explicitly in Table I in the Appendix, when comparing clean surfaces and those with water, we always observe the following two trends: (1) There is only a small difference between friction at the steps versus terraces when clean, while when water is present, friction at steps is much higher; and (2) the slope of the friction versus normal force

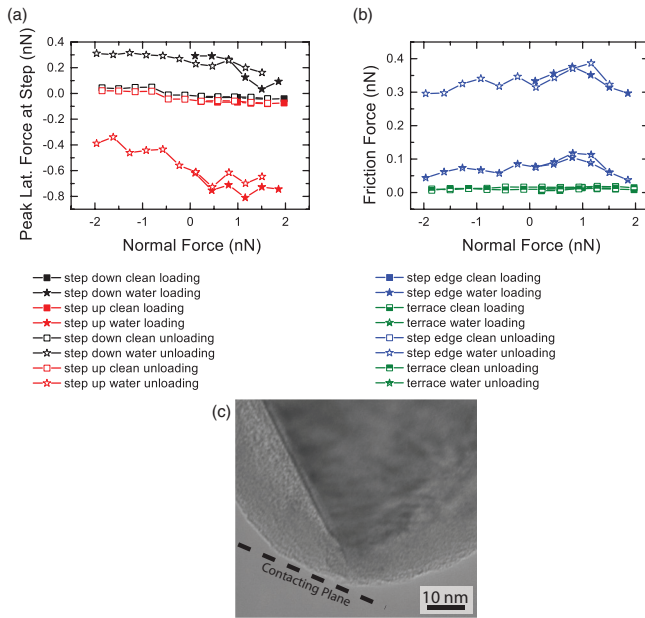


FIG. 4. (Color online) Results from a repeated experiment with a different tip having a larger contacting asperity. The load dependence of (a) the peak lateral force and (b) friction force recorded at the step edge measured on both the clean (HV) surface and with water present (dry nitrogen conditions) with the same tip. Solid data points were taken during loading and open data points were taken during unloading. Red (black) friction data always indicate step-up (step-down) measurements. (d) TEM image of the tip apex showing that the tip has a 29 ± 1 nm radius. The plane at which the surface contacts the tip asperity is marked by a dashed line.

data at steps for all tips is significantly enhanced when water is present when compared to clean surfaces. While caution should be used when comparing data from different tips, the trend of observing a higher slope when water is present versus the clean case is consistent across all tips.

B. Simulation results

To explore the origins of the friction response measured at atomic steps, we conducted MD simulations matching experimental conditions as closely as possible within computational constraints. First, we modeled the tip sliding over a step edge on a clean surface.²⁶ Figure 5(a) shows a lateral force profile for a sliding tip on this clean surface. Consistent with experiments, the lateral force peak at the step edge is negative in both the forward and reverse directions, due to the geometric effect. In Fig. 5(c), the dependence of the peak lateral force on normal force in both step-up (red squares) and step-down (black squares) directions shows a similar negative trend, as in the experiments, as expected for the geometric effect of steps. Also similar to experiments, Fig. 5(d) shows higher friction occurs at the step edge (blue squares) compared to the terrace (green squares). Consistent trends were observed for tip radii varying between 2 and 8 nm.

As discussed above, the experimental results suggest that water adsorption at steps increases frictional dissipation. To test this, we introduced 456 water molecules that were evenly distributed across the HOPG surface. Shortly after

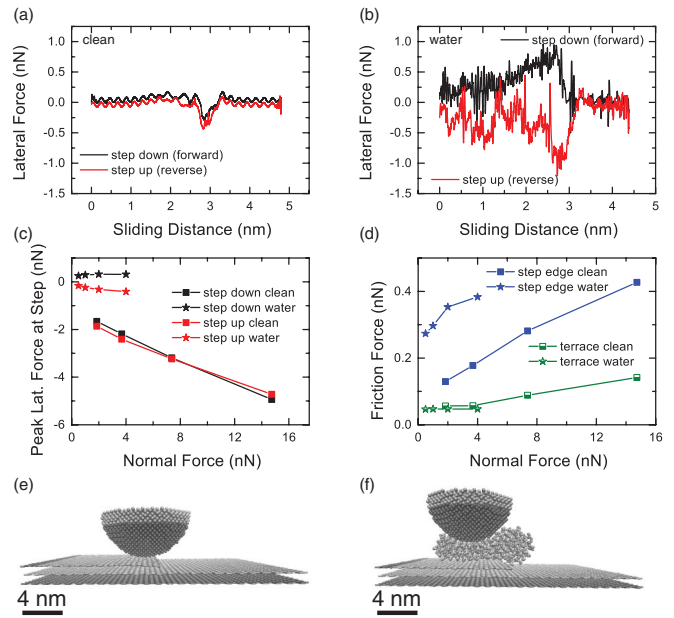


FIG. 5. (Color online) MD simulations of sliding on HOPG at steps. Lateral force line profiles acquired on (a) a clean surface (normal force = 0 nN) and (b) with two layers of water molecules in the contact zone (normal force = 0 nN). Red (black) data always indicate step-up (step-down) measurements. The load dependence of (c) peak lateral force and (d) friction measured on both the clean surface and with two layers of water molecules in the contact zone. Illustrations of the 2 nm radius tip sliding over the graphite substrate on (e) a clean surface and (f) with water molecules in the contact zone. (a), (b), (e), and (f) are from simulations conducted at 300 K. The load dependence results in (c) and (d) were performed at 10 K.

the simulation began, the water molecules accumulated to form a stable droplet [Fig. 5(f)].²⁶ This droplet is strongly attracted to the step edge and remains there, regardless of the tip’s movement. Figure 5 shows the lateral forces when scanning in the presence of these water molecules. There is a significant increase in friction at the step edge, consistent with the experimental results. The trends in the variation of peak lateral force [Fig. 5(c)] and friction [Fig. 5(d)] versus load are not only qualitatively consistent between the simulation and experimental results [Figs. 2(c) and 2(d)], but in fact friction forces on the terrace agree within a factor of 2 for comparable loads. Furthermore, the MD results show that the addition of a small amount of water on the surface does not strongly influence the load dependence of friction on the terrace, consistent with the experimental results.

IV. DISCUSSION

These results help explain ambiguous or inconsistent reports of lateral forces at atomic steps that are often discussed in terms of the Schwoebel-Ehrlich barrier. The Schwoebel-Ehrlich barrier is defined as the higher local surface energy at atomic steps that arises from the lower coordination of atoms at the step edge, leading to an enhanced interaction energy with single diffusing atoms or molecules. Unlike single atoms or molecules, the potential used in atomic friction models must account for the many-atom tip-sample interaction. The

small additional friction observed at clean steps in both experiment and simulation on clean surfaces here and in previous reports^{6–8} is a result of the enhanced interaction between the high energy step atoms and the tip, essentially a Schwoebel-Ehrlich barrier for tips, as discussed several times before.^{7,9} Given this proposition, the energy landscape must be influenced by the tip properties. However, in MD simulations, we did not observe higher friction at atomic steps compared to terraces on clean surfaces, regardless of the tip size. In experiments, while higher friction was sometimes seen at steps compared to terraces in clean conditions [Fig. 4(d)], in most cases there was little to no resolvable difference [Figs. 2(b), 7(a), and 7(c)]. Furthermore, in both MD simulations and experiments, we did not observe a peak lateral force more resistive than the average lateral force observed on the flat terrace on clean surfaces. On the other hand, we consistently observe additional friction at steps in experiments and simulations conducted with water present, regardless of tip radius. The MD simulations demonstrate that the interaction between the Schwoebel-Ehrlich barrier, the water molecules, and the tip result in additional dissipation, yielding consistent results with all previously published ambient friction experiments,^{9–11} and with our own results when water was present.

All other studies examining friction at steps have been conducted in UHV conditions.^{6–8} We hypothesize that the cases of significantly enhanced friction observed at atomic steps in some of these results is due to the tip *shape*, rather than size. More specifically, Steiner *et al.* suggested that worn tips resulted in enhanced friction at steps in UHV.⁷ In systematic studies of tip wear against atomically flat surfaces, tip apices have been seen to become flat (i.e., truncated), as opposed to remaining round with an increasing radius.²⁷ Given the wide size range of round tips, rather than flat tips, examined on clean surfaces in both experiments and simulations here, which also all yielded a geometry-dominated behavior (moderate to no friction enhancement at the step), our results suggest that tip shape as opposed to tip size results in the enhancement of friction at atomic steps. To be more explicit, we propose that the mechanism by which friction at atomic steps is increased in the presence of water is different than what is proposed by Steiner *et al.*⁷ Our MD simulations of tips having a flattened (i.e., truncated) apex suggest that tip trajectory is responsible for the enhanced friction observed at a step edge in UHV or clean surfaces.²⁸ Although tip images were not obtained in any other study of atomic friction experiments of step edges, the large width (~ 100 nm) of the single atomic step edges in the lateral force images of Müller *et al.*⁸ and wide step widths seen in other UHV studies⁶ suggest that the observed increased friction behavior at steps in vacuum results from tips having a flattened apex. Further work with systematically varied tip shapes is required to verify this hypothesis.

Finally, graphite steps are observed to buckle slightly as the tip slides in the step-up direction, as shown in MD simulations on clean surfaces²⁹ and as reported in certain AFM experiments.¹¹ Our MD simulations on clean surfaces show that this Ångströms step buckling is a few Ångströms in magnitude, and has little influence on the friction force. This was determined by observing almost no change in the friction forces that arose when the step atoms were artificially fixed in place compared to when they were allowed to freely move.

This result shows that the slightly enhanced friction observed on clean surfaces arises from the variation in the surface energy landscape at steps and not buckling of the step edge, as was proposed by Ref. 11. However, in simulations with water present, we observe almost no movement of the step when the step atoms are allowed to move. Further studies are required to understand this in full. However, the observed buckling of the step edges on clean surfaces could be a precursor mechanism for the increased wear of graphite that is known to occur in dry environments.¹⁵

V. CONCLUSIONS

We have shown that, although the friction behavior on HOPG terraces is not strongly affected by the environment, the presence of even a small amount of water at atomic step edges significantly increases friction. Separation of the frictional dissipation observed as the tip slides from the terrace over the step and the instantaneous lateral forces measured during this transition have uncovered the mechanism by which a sliding, nanoscale asperity experiences additional friction at atomic steps on graphite. The lateral force at a step edge on clean HOPG surfaces is slightly more dissipative due to the effect of the Schwoebel-Ehrlich barrier on the tip, but far larger friction occurs at step edges when water is adsorbed at the step. In fact, for each tip used in experimental measurements, similar trends can be observed, including a small decrease in the friction measured at the step versus the terrace and a decrease in the slope of the friction versus normal force data at steps when comparing surfaces when water is present to clean surfaces. Also in experiments, we observe a transition from enhanced friction when water is present, to friction dominated by the geometry of the tip when the sample is clean (no water adsorbed). MD simulations including adsorbed water molecules produced consistent results.

ACKNOWLEDGMENTS

This work was funded by the US National Science Foundation under Grants No. CMMI-1068552 and CMMI-1068741. We are grateful to H. Hölscher and Q. Li for insightful discussions, to T. D. B. Jacobs, G. Wabiszewski, and V. Vahdat for acquiring the TEM images of the AFM probes, and to F. Mangolini for acquiring the XPS spectra. P.E. would like to acknowledge financial support from the Natural Sciences and Engineering Research Council (NSERC) of Canada.

APPENDIX

This Appendix includes additional experimental data acquired in N_2 without prior vacuum exposure (i.e., with water present) (Fig. 6) and under HV or clean conditions (Fig. 7) using a modified procedure to the one outlined in the experimental section, which is explained further below. For each environment, results from two additional tips are given, demonstrating the repeatability of the results provided in the main body of this paper. In each figure, the normal force dependence of the friction force at the step edge and on the terrace, as well as the normal force dependence of the peak lateral forces measured as the tip slid over the step, are plotted in a single graph using the same color (symbol) scheme as

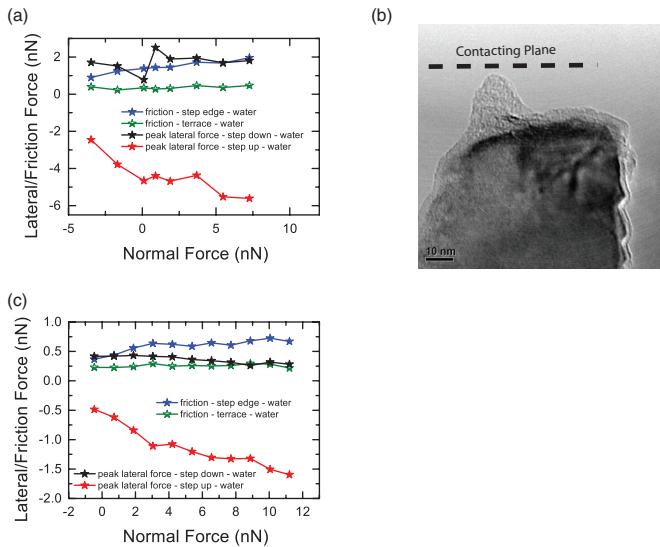


FIG. 6. (Color online) Measurements of friction made with water present (in dry nitrogen conditions) for two different tips. The load dependence of the peak lateral forces and friction forces are shown in (a) for tip 1 and (c) for tip 2. Red (black) data always indicate step-up (step-down) measurements. Only unloading data is presented in (a) and (c). Blue (green) data always indicate friction measurements on steps (terraces). A TEM image of tip 1 is shown in (b), which has a radius of 5 ± 3 nm. The plane the surface contacts the asperity of the tip is marked by a dashed line. Tip 1 was used to acquire the data shown in Fig. 2(h).

before (black for step down, red for step up, green for friction measured on flat terraces, blue for friction measured at the step

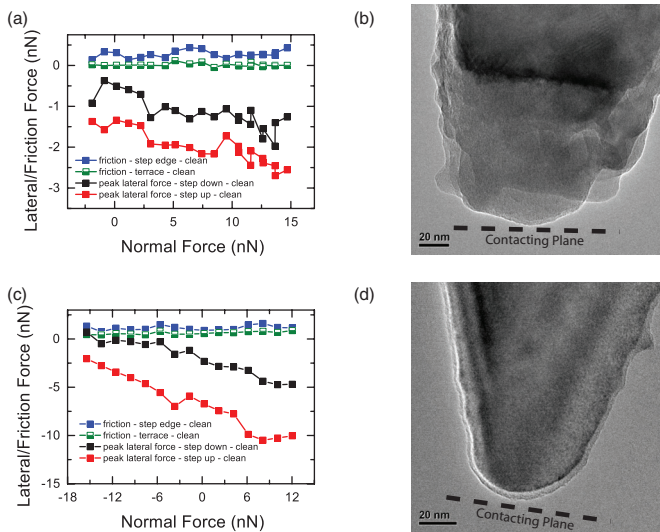


FIG. 7. (Color online) Measurements of friction made on the clean surface (under HV conditions) for two different tips. The load dependence of the peak lateral forces and friction forces are shown in (a) for tip 1 and (c) for tip 2. Red (black) data always indicate step-up (step-down) measurements. Only unloading data is presented in (a) and (c). Blue (green) data always indicate friction measurements on steps (terraces). TEM images of tips 1 and 2 are given in (b) and (d), respectively. Tip 1 has a radius of 38 ± 5 nm and tip 2 has a radius of 26.2 ± 0.5 nm.

edge, squares for experiments conducted under HV conditions, and stars for experiments conducted under N_2 conditions). These friction and lateral force results are displayed beside a TEM image of the contacting asperity of the tip used to acquire the data. In some of the experimental data shown here, better and more clearly varying trends in the dependence of friction at step edges and on terraces, as well as the dependence of the lateral forces at step edges, are evident. However, the results given in this Appendix were obtained in two different AFM systems (one system is contained in an environmental chamber, and the other one is the AFM used to acquire all data in the main body of the paper, and was kept under vacuum conditions for these results). Given this issue, we could not have the used same tip in both environments, resulting from experimental constraints.

In Fig. 6, data was acquired by freshly cleaving the HOPG sample in air, as described in the experimental section. The sample was then immediately placed inside the vacuum chamber of an RHK 350 UHV AFM system which was purged with N_2 , using the same dry N_2 source as described in the experimental section, where the low $<2\%$ humidity value quoted in the experimental section was measured. Friction experiments were conducted on the sample inside the chamber within a few hours. The force constants of the cantilevers used in this system was calculated using the Sader method,²⁰ exactly as discussed previously in the experimental section. The same selection criteria for choosing the HOPG steps to be examined was used as in the previous sections of the paper. In every test conducted in this AFM in this dry N_2 environment, friction properties of atomic steps showed the same characteristics previously shown in the dissipation-dominated case. In particular, we observe (1) the strong geometric effect in the lateral force in the step-up direction, and (2) higher friction overall and a stronger dependence of friction on normal force for steps versus terraces.

In Fig. 7, data was acquired by freshly cleaving the HOPG sample as described in the experimental section and then placing the sample in the load lock of the RHK 750 UHV AFM system described in the methods section. The load lock was pumped down immediately, reaching HV pressures in approximately 1 h. The sample was than transferred into the UHV chamber, where the pressure was less than 1×10^{-7} Torr. Friction experiments were then conducted only under these HV conditions. Given the absence of a damping fluid medium in vacuum conditions, the Sader method cannot be used to calibrate cantilevers whose resonant frequencies are measured under vacuum. In this case, the force constants of the cantilevers used in this system were calibrated using the beam geometry method, where the resonant frequency of the first normal bending mode was used to determine the thickness of the cantilever.³⁰ After determining the thickness of the cantilever, the normal bending and lateral twisting stiffnesses can be determined. The remaining calibration steps used in determining the force data were performed in the same manner as described in the methods section. The same selection criteria for choosing HOPG steps to be examined was used as in the previous sections of this paper. In every test conducted in this AFM under HV conditions, friction properties of atomic steps showed the same characteristics previously shown in the geometry-dominated case.

TABLE I. Values of the slopes obtained from linear fits to each of the friction force versus normal force plots contained within this paper.

| Figure number | Area on the surface | Surface condition | Slope value |
|----------------|---------------------|-------------------|---------------------|
| 2(c) | Terrace | Clean | 0.0040 ± 0.0008 |
| | | Water present | 0.007 ± 0.004 |
| | Step edge | Clean | 0.02 ± 0.02 |
| | | Water present | 0.04 ± 0.01 |
| 4(c) | Terrace | Clean | 0.0008 ± 0.0005 |
| | | Water present | 0.013 ± 0.005 |
| | Step edge | Clean | 0.0023 ± 0.0005 |
| | | Water present | 0.017 ± 0.006 |
| 6(a) | Terrace | Water present | 0.013 ± 0.008 |
| | Step edge | Water present | 0.087 ± 0.009 |
| 6(c) | Terrace | Water present | 0.002 ± 0.002 |
| | Step edge | Water present | 0.023 ± 0.005 |
| 7(a) | Terrace | Clean | -0.001 ± 0.002 |
| | Step edge | Clean | 0.004 ± 0.004 |
| 7(c) | Terrace | Clean | 0.012 ± 0.003 |
| | Step edge | Clean | 0.008 ± 0.007 |
| Average values | Terrace | Clean | 0.0040 ± 0.0009 |
| | | Water present | 0.009 ± 0.003 |
| | Step edge | Clean | 0.009 ± 0.005 |
| | | Water present | 0.042 ± 0.004 |

In both Figs. 6 and 7, great care was taken to prevent damage to the tip while searching for single atomic steps that were oriented near 90° with respect to the fast scan direction, and then all experiments were stopped once the load dependence data was taken. As such, we can assume the tip asperity captured in TEM images is representative of the tip shape

during experiments. We never saw a change in the friction properties measured at atomic steps resulting from tip wear, as discussed in Steiner *et al.*⁷

Finally, in Table I we present the slopes of best-fit straight lines to the unloading portion of the friction versus normal force data for all tips tested.

*amartini@ucmerced.edu

†carpick@seas.upenn.edu

¹C. M. Mate, G. M. McClelland, R. Erlandsson, and S. Chiang, *Phys. Rev. Lett.* **59**, 1942 (1987).

²I. Szlufarska, M. Chandross, and R. W. Carpick, *J. Phys. D* **41**, 123001 (2008).

³Y. Dong, Q. Li, and A. Martini, *J. Vac. Sci. Technol. A* **31**, 030801 (2013).

⁴Q. Li, Y. Dong, D. Perez, A. Martini, and R. W. Carpick, *Phys. Rev. Lett.* **106**, 126101 (2011).

⁵N. N. Gosvami, M. Feldmann, J. Peguiron, M. Moseler, A. Schirmeisen, and R. Bennewitz, *Phys. Rev. Lett.* **107**, 144303 (2011).

⁶E. Meyer, R. Lüthi, M. Howald, M. Bammerlin, M. Guggisberg, and H.-J. Güntherodt, *J. Vac. Sci. Technol. B* **14**, 1285 (1996).

⁷P. Steiner, E. Gnecco, F. Krok, J. Budzioch, L. Walczak, J. Konior, M. Szymonski, and E. Meyer, *Phys. Rev. Lett.* **106**, 186104 (2011).

⁸T. Müller, M. Lohrmann, T. Kässer, O. Marti, J. Mlynek, and G. Krausch, *Phys. Rev. Lett.* **79**, 5066 (1997).

⁹H. Hölscher, D. Ebeling, and U. D. Schwarz, *Phys. Rev. Lett.* **101**, 246105 (2008).

¹⁰D. R. Baselt and J. D. Baldeschwieler, *J. Vac. Sci. Technol. B* **10**, 2316 (1992).

¹¹D. P. Hunley, T. J. Flynn, T. Dodson, A. Sundararajan, M. J. Boland, and D. R. Strachan, *Phys. Rev. B* **87**, 035417 (2013).

¹²H. Shindo, M. Ohashi, O. Tateishi, and A. Seo, *J. Chem. Soc., Faraday Trans.* **93**, 1169 (1997).

¹³C. Sommerhalter, T. W. Matthes, T. Glatzel, A. Jäger-Waldau, and M. C. Lux-Steiner, *Appl. Phys. Lett.* **75**, 286 (1999).

¹⁴C. Greiner, J. R. Felts, Z. Dai, W. P. King, and R. W. Carpick, *Nano Lett.* **10**, 4640 (2010).

¹⁵R. H. Savage, *J. Appl. Phys.* **19**, 1 (1948).

¹⁶X. Feng, S. Maier, and M. Salmeron, *J. Am. Chem. Soc.* **134**, 5662 (2012).

¹⁷J. Hu, X.-D. Xiao, and M. Salmeron, *Appl. Phys. Lett.* **67**, 476 (1995).

¹⁸F. Mangolini, J. Åhlund, G. E. Wabiszewski, V. P. Adiga, P. Egberts, F. Streller, K. Backlund, P. G. Karlsson, B. Wannberg, and R. W. Carpick, *Rev. Sci. Instrum.* **83**, 093112 (2012).

¹⁹J. Liu, J. K. Notbohm, R. W. Carpick, and K. T. Turner, *ACS Nano* **4**, 3763 (2010).

²⁰C. P. Green, H. Lioe, J. Cleveland, R. Proksch, P. Mulvaney, and J. E. Sader, *Rev. Sci. Instrum.* **75**, 1988 (2004).

- ²¹I. Horcas, R. Fernández, J. M. Gómez-Rodríguez, J. Colchero, J. Gómez-Herrero, and A. M. Baro, *Rev. Sci. Instrum.* **78**, 013705 (2007).
- ²²Y. Niimi, T. Matsui, H. Kambara, K. Tagami, M. Tsukada, and H. Fukuyama, *Phys. Rev. B* **73**, 085421 (2006).
- ²³S. J. Stuart, A. B. Tutein, and J. A. Harrison, *J. Chem. Phys.* **112**, 6472 (2000).
- ²⁴W. L. Jorgensen, J. Chandrasekhar, J. D. Madura, R. W. Impey, and M. L. Klein, *J. Chem. Phys.* **79**, 926 (1983).
- ²⁵G. Haugstad, W. L. Gladfelter, and E. B. Weberg, *Langmuir* **9**, 3717 (1993).
- ²⁶See Supplemental Material at <http://link.aps.org/supplemental/10.1103/PhysRevB.88.035409> for movies of the MD simulations on clean surfaces and on surfaces with water present. The applied load in each case was 0 nN, as stated in the methods section.
- ²⁷J. Liu, D. S. Grierson, N. Moldovan, J. Notbohm, S. Li, P. Jaroenapibal, S. D. O'Connor, A. V. Sumant, N. Neelakantan, J. A. Carlisle, K. T. Turner, and R. W. Carpick, *Small* **6**, 1140 (2010).
- ²⁸Z. Ye, A. Otero-de-la Roza, E. R. Johnson, and A. Martini, *Appl. Phys. Lett.* (to be published).
- ²⁹Y. Dong, X.-Z. Liu, P. Egberts, Z. Ye, R. W. Carpick, and A. Martini, *Tribol. Lett.* **50**, 49 (2013).
- ³⁰E. Meyer, H. J. Hug, and R. Bennewitz, *Scanning Probe Microscopy: The Lab on a Tip* (Springer, Berlin, 2004).